Estudio experimental y teórico de la cinética y mecanismo de la eliminación unimolecular y homogénea del ácido 2-Furoico en fase gaseosa

ARTICLE

Source: OAI

3 AUTHORS, INCLUDING:

Gabriel Chuchani
Venezuelan Institute for Scientific Research
245 PUBLICATIONS   **1,212** CITATIONS

SEE PROFILE

Tania Cecilia Cordova-Sintjago
University of Florida
99 PUBLICATIONS   **256** CITATIONS

SEE PROFILE

Experimental and Theoretical Study of the Homogeneous, Unimolecular Gas-Phase Elimination Kinetics of 2-Furoic Acid

BEATRIZ C. RAMÍREZ,[1] ROSA M. DOMÍNGUEZ,[2] ARMANDO HERIZE,[2] MARÍA TOSTA,[2] TANIA CORDOVA,[1] GABRIEL CHUCHANI[2]

[1]Laboratorio de Fisico-Química Orgánica. Escuela de Química, Facultad de Ciencias, Universidad Central de Venezuela, Caracas 1020-A, Venezuela

[2]Centro de Química, Instituto Venezolano de Investigaciones Científicas (IVIC), Apartado 21827, Caracas 1020-A, Venezuela

ABSTRACT: The kinetics of the gas-phase elimination kinetics of CO_2 from furoic acid was determined in a static system over the temperature range 415–455°C and pressure range 20–50 Torr. The products are furan and carbon dioxide. The reaction, which is carried out in vessels seasoned with allyl bromide and in the presence of the free-radical suppressor toluene and/or propene, is homogeneous, unimolecular, and follows a first-order rate law. The observed rate coefficient is expressed by the following Arrhenius equation: $\log k_1 (s^{-1}) = (13.28 \pm 0.16) - (220.5 \pm 2.1) \text{ kJ mol}^{-1} (2.303 \text{ RT})^{-1}$. Theoretical studies carried out at the B3LYP/6-31++G** computational level suggest two possible mechanisms according to the kinetics and thermodynamic parameters calculated compared with experimental values. © 2007 Wiley Periodicals, Inc. Int J Chem Kinet 39: 298–306, 2007
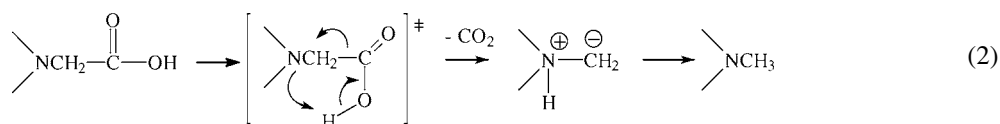
INTRODUCTION

Both experimental and theoretical studies on the gas-phase elimination of several α- or 2-substituted aliphatic carboxylic acids suggest the mechanism of decarbonylation [1–7], as described in reaction (1)
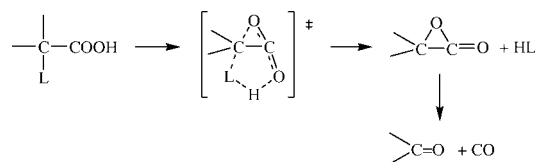
L = Leaving Group: Cl, Br, OH, OR, OPh, OAc.

(1)

It is interesting to note that the atom of the substituent directly attached at the α- or 2-carbon of the COOH group is a heteroatom. However, when a nitrogen atom is at the 2-position of the carboxylic acid, for example, an α-amino acid (such as *N*,*N*-dimethylglycine [8] or *N*-phenylglycine [9]), a gas-phase decarboxylation process takes place [reaction (2)].

and the purity of this substrate were verified by GC-MS (Saturn 2000, Varian, with a DB-5MS capillary column 30 m × 0.25 mm i.d., 0.25-μm film thickness). The quantitative analysis of the product CO_2 was carried out using a gas chromatograph (Varian 3600X) with a thermal conductivity detector (capillary column: GS-Q, 30 m × 0.53 mm i.d., Helium gas carrier).

$$\text{(2)}$$

Consequently, the mechanism described in reaction (2) differs both experimentally and theoretically from that reported for the gas-phase elimination of several types of 2-substituted carboxylic acids.

The effect of a heteroaromatic group attached at the acid side of a carboxylic acid in the gas-phase elimination reaction has scarcely been reported, particularly when the heteroatom is located at the 2-carbon with respect to the COOH group. In this respect, a few years ago, the homogeneous, unimolecular gas-phase elimination kinetics of picolinic acid was found to decarboxylate at very low temperature [10]. The mechanism of decomposition of this acid was thought to be polar in nature, as depicted in reaction (3):

$$\text{(3)}$$
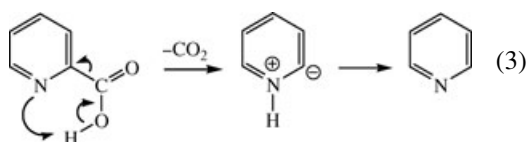
Some heteroaromatic molecules have double bond characteristics and are less aromatic than pyridine, for example, furan. To understand the double bond characteristics of these compounds, the present work was aimed at examining the gas-phase elimination kinetics of 2-furoic acid and to report on a combination of kinetic experiments and theoretical studies of the said substrate. The intention was to obtain the kinetic parameters and to characterize the potential energy surface (PES) in order to establish the molecular mechanism of the elimination reaction.

EXPERIMENTAL

The substrate 2-furoic acid acquired from Aldrich (of 98.8% purity) was used. The identification of products

Kinetic Studies

The kinetic experiments were performed in a static reaction system previously reported [11–13]. The rate coefficients were determined manometrically. The temperature was controlled by a Shinko DC–PS resistance thermometer controller and maintained with ±0.2°C and measured with a calibrated iron–constantan thermocouple. No temperature gradient was found along the reaction vessel. The substrate was dissolved in dioxane and injected (0.05–0.1 mL) directly into the reaction vessel with a syringe through a silicone rubber septum.

COMPUTATIONAL METHOD AND MODEL

The kinetics and mechanisms of 2-furoic acid gas-phase elimination to give furan and carbon dioxide were investigated by means of electronic structure calculations using DFT B3LYP/6-31++G(d,p) as implemented in Gaussian 98W [14]. Structures of the reactants and products were optimized at each theory level, and transition states were searched and optimized using synchronous transit (QST2, QST3) methodologies. The Berny analytical gradient optimization routines were used. The requested convergence on the density matrix was 10^{-9} atomic units, the threshold value for maximum displacement was 0.0018 Å, and that for maximum force was 0.00045 Hartree/Bohr. The nature of the stationary points was established by calculating and diagonalizing the Hessian matrix (force constant matrix). Transition state (TS) structures were characterized by means of normal-mode analysis. The transition vector (TV) associated with the unique imaginary frequency, that is, the eigenvector associated with the unique negative eigenvalue of the force constant matrix, has been characterized.

Thermodynamic quantities such as the zero-point vibrational energy (ZPVE), temperature corrections

$E(T)$, and absolute entropies $S(T)$ were obtained by frequency calculations and, consequently, the rate coefficient was estimated assuming the transmission coefficient is equal to 1. Temperature corrections and absolute entropies were obtained assuming ideal gas behavior from the harmonic frequencies and moments of inertia by standard methods [15] at average temperature and pressure values within the experimental range. Scaling factors for frequencies and zero-point energies are taken from the literature [16].

The first-order rate coefficient $k(T)$ was calculated using the TST [14] and assuming that the transmission coefficient is equal to 1, as expressed in the following relation:

$$k(T) = (KT/h) \exp\left(-\Delta G^{\#}/RT\right)$$

where $\Delta G^{\#}$ is the Gibbs free energy change between the reactant and the transition state and K and h are the Boltzmann and Planck constants, respectively.

$\Delta G^{\#}$ was calculated using the following relations:

$$\Delta G^{\#} = \Delta H^{\#} - T\Delta S^{\#}$$

and

$$\Delta H^{\#} = V^{\#} + \Delta(ZPVE) + \Delta E(T)$$

where $V^{\#}$ is the potential energy barrier and $\Delta(ZPVE)$ and $\Delta E(T)$ are the differences of ZPVE and temperature corrections between the TS and the reactant, respectively.

Frequency calculations were made at average experimental conditions ($T = 435°C$, $P = 0.105$ atm), at the same level of optimization as used in the theoretical calculations. Thermodynamic quantities such as the zero-point vibrational energy (ZPVE), temperature corrections ($E(T)$), energy, enthalpy, and free energies were obtained from vibrational analysis. Entropy values were calculated from vibrational analysis using the factor C^{exp} of Chuchani–Cordova [17].

RESULTS AND DISCUSSION

The elimination reaction of 2-furoic acid in a static system, seasoned with allyl bromide and in the presence of the free-radical inhibitor toluene and/or propene was determined over the temperature range 415–455°C and the pressure range 20–120 Torr. The decomposition products are furan and CO_2 [reaction (4)]. The

$$\text{(furan-COOH)} \longrightarrow \text{(furan)} + CO_2 \qquad (4)$$
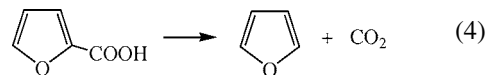
stoichiometry (4), up to 85% reaction, was verified by comparing between the carbon dioxide formation with the pressure increase of the substrate decomposition (Table I). To determine the influence of the surface area on the rate of elimination (4), several runs were carried out in a vessel with a surface-to-volume ratio six times greater than that of the normal vessel (Table II). The packed and unpacked clean Pyrex vessels had a marked effect on the rates. However, the packed and unpacked Pyrex vessels seasoned with allyl bromide appears to have no effect on rates.

Different proportions of the free-radical inhibitor toluene and/or propene in the elimination process are shown in Table III. 2-Furoic acid, in seasoned vessels, had to be carried out in the presence of at least twice the amount of the inhibitor toluene and/or propene in order to prevent any radical reaction. No induction period was observed and the rates were reproducible with a standard deviation <5% at a given temperature. (The precision of manometric measurements is ±0.5 mm.)

The first-order rate coefficients of this elimination calculated from $k_1 = (2.303/t) \log P_0/(2P_0 - P_t)$ were found to be independent to initial pressures (Table IV). A plot of $\log(2P_0 - P_t)$ against time t gave a good straight line up to 85% reaction. The variation of the rate coefficients with temperature and the corresponding Arrhenius equation is given in Table V (90% confidence coefficient from least-squares procedure). The Arrhenius plot is described in Fig. 1.

With these available experimental kinetic and thermodynamic parameters (Table VI), together with a theoretical study, it may be possible to consider a reasonable mechanism for the gas-phase elimination of 2-furoic acid.
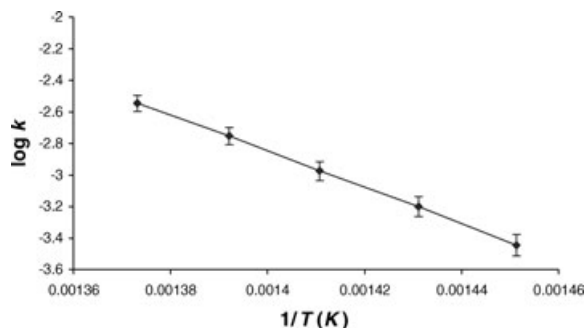

Figure 1   Arrhenius plot of the elimination kinetics of 2-furoic acid. Slope $= -11519.4$, intercept $= 13.28$, SD $= 0.006$, $r = 0.9999$.

Table I Stoichiometry of the Reaction

Substrate	Temperature (°C)	Parameter					Value
2-Furoic acid	435	Time (min)	5	10	15	20	26
		Reaction (%) (pressure)	28.5	45.1	62.1	74.4	85.3
		CO_2 (%) (GLC)	28.2	46.0	60.0	74.6	84.1

Table II Homogeneity of the Reaction

Substrate	Temperature (°C)	S/V (cm^{-1})^a	$10^4 k_1$ (s^{-1})^b	$10^4 k_1$ (s^{-1})^c
2-Furoic acid	415.6	1	12.96 ± 0.30	3.58 ± 0.10
		6	13.27 ± 0.33	3.42 ± 0.21

^{a} S = surface area (cm^2); V = volume (cm^3).
^{b} Clean Pyrex vessel.
^{c} Vessel seasoned with allyl bromide.

Table III Effect of the Free-Radical Suppressor Toluene and/or Propene on Rates

Substrate	Temperature (°C)	P_0(Torr)	P_i (Torr)	P_i/P_0	$10^4 k_1$(s^{-1})
2-Furoic acid^a	435.7	40.0	—	—	9.52
		56.5	40.0	0.7	9.45
		43.0	60.0	1.4	10.42
		34.0	74.0	2.2	10.52
		38.5	108.0	2.8	10.48
		42.0	134.0	3.2	10.69
		36.0	130.5	3.6	10.46

P_0 = pressure of the substrate; P_i = pressure of the inhibitor.
^{a} Vessel seasoned with allyl bromide.

Table IV Variation of the Rate Coefficients With Initial Pressure^{a,b}

| Substrate	Temperature (°C)	Parameters		Value			
2-Furoic acid	445.2	P_0 (Torr)	22	25	29.5	38.5	46
		$10^4 k_1$ (s^{-1})	17.49	17.68	17.67	17.68	17.69

^{a} Vessel seasoned with allyl bromide.
^{b} In the presence of the inhibitor toluene and/or propene.

Table V Temperature Dependence of the Rate Coefficients

Substrate	Parameters			Value		
2-Furoic acid	Temp. (°C)	415.9	425.6	435.7	445.2	455.1
	$10^4 k_1$ (s^{-1})	3.58 ± 0.10	6.31 ± 0.09	10.60 ± 0.12	17.64 ± 0.09	28.53 ± 0.06

Rate equation $\log k_1$ (s^{-1}) = $(13.28 \pm 0.16) - (220.5 \pm 2.1)$ kJ mol^{-1} $(2.303RT)^{-1}$; $r = 0.9998$.

Table VI Kinetic and Thermodynamic Parameters at 435.0°C

Substrate	$10^4 k_1$ (s^{-1})	E_a (kJ mol^{-1})	$\log A$ (s^{-1})	$\Delta S^{\ddagger}$ (J mol^{-1} K^{-1})	$\Delta H^{\ddagger}$ (kJ mol^{-1})	$\Delta G^{\ddagger}$ (kJ mol^{-1})
2-Furoic acid	10.27	220.5 ± 2.1	13.28 ± 0.16	-6.2	214.6	219.0

Mechanism 1:
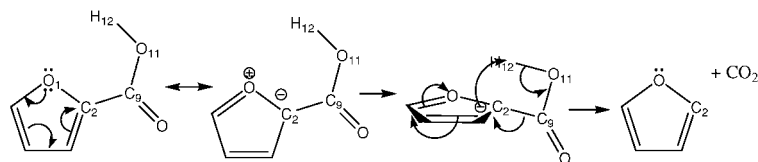
Mechanism 2:
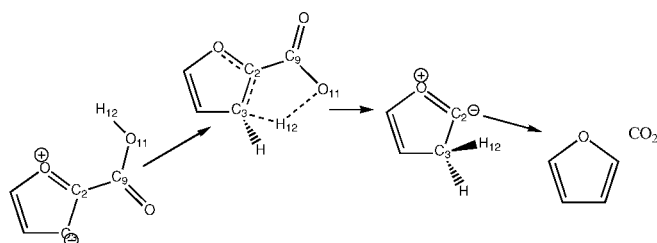
Scheme 1   Two mechanisms were found for 2-furoic acid thermal decomposition.

THEORETICAL RESULTS

Kinetic and Thermodynamic Parameters

The gas-phase thermal decomposition of 2-furoic acid was studied by theoretical calculations of the electronic structure. Two possible transition states, four- and five-membered ring structures, were found connecting the reactant and products. The two mechanisms were examined to establish the kinetic and thermodynamic parameters to be compared to the experimental counterparts. The two possible mechanisms are shown in Scheme 1.

Results from B3LYP/6-31++G** calculations for mechanisms 1 and 2 are shown in Tables VII and VIII. Calculated parameters of the two mechanisms were compared with experimental values, showing better accord for mechanism 1.

Transition States and Mechanisms

The gas-phase elimination reaction of 2-furoic acid can occur through two transition states. Transition states were verified by means of IRC calculations. The transition state for mechanism 1 (TS-I) is a cyclic four-membered structure as suggested by values of log A of 13.07–13.64 [18]. TS-I geometries are almost identical for all levels of theory, both in distances and angles between the atoms involved in the reaction (O1, C2, C3, C9, O11, and H12), with the hydrogen being transferred (H12) midway between the carbon C2 and the oxygen O11 (Fig. 2, Scheme 2). The four atoms involved in the TS structure lie in a different plane with respect to the furan ring plane. Structural parameters for the four-membered ring TS are shown in Table IX.

The TS-I dihedral angle C_2—C_9—O_{11}—H_{12} shows that the four atoms involved in the TS are in a plane

Table VII   Kinetics and Thermodynamic Parameters for Thermal Decomposition of 2-Furoic Acid by Mechanism 1 at 435°C and 0.105 atm

Level of Theory	$\Delta H^{\neq}$(kJ mol^{-1})	$\Delta G^{\neq}$(kJ mol^{-1})	$\Delta S^{\neq}$(J K^{-1} mol^{-1})	$E_a^{\neq}$(kJ mol^{-1})	log A	k (s^{-1})
B3LYP/6-31G++G**	232.2	232.4	−0.1	238.1	13.60	1.08
Experimental	214.6	219.0	−6.2	220.5	13.28	10.27

Table VIII   Kinetics and Thermodynamic Parameters for Thermal Decomposition of 2-Furoic Acid by Mechanism 2 at 435°C and 0.105 atm

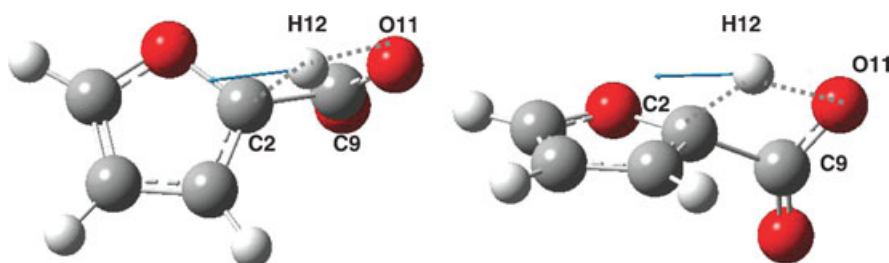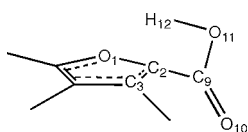| Level of Theory	$\Delta H^{\neq}$(kJ mol^{-1})	$\Delta G^{\neq}$(kJ mol^{-1})	$\Delta S^{\neq}$(J K^{-1} mol^{-1})	$E_a^{\neq}$(kJ mol^{-1})	log A	k (s^{-1})
B3LYP/6-31++G**	242.0	241.1	1.3	247.9	13.67	0.242
Experimental	214.6	219.0	−6.2	220.5	13.28	10.27

Figure 2   Two views of the four-membered ring TS structure found for mechanism 1, showing the transition vector. [Color figure can be viewed in the online issue, which is available at www.interscience.wiley.com.]
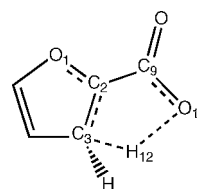

Scheme 2

Scheme 3

while the dihedral angle O_1—C_2—C_9—O_{11} indicates that the four-membered ring structure is at approximately 120° from the plane of the furan ring. The process is concerted in the sense that O11—H12 and C2—C9 bond distances increase, showing breaking of these bonds (0.970–1.441 Å in TS-I and 1.472–1.630 Å in TS-I, respectively). The C9—O11 and C2—O1 bond distances reveal changes of bond order (1.211–1.288 Å in TS-I and 1.377–1.404 Å in TS-I, respectively), while the C2—H12 distance decreases, indicating bond formation. The transition vector TV associated with the imaginary frequency characteristic of the TS shows that the process is dominated by the elongation of the O11—H12 bond.

The transition state for mechanism 2 (TS-II), which is a cyclic five-membered structure (Fig. 3, Scheme 3), is also in accord with the log A values (12.70–13.94) [19]. Intrinsic reaction coordinate (IRC) calculations were performed to verify that this TS connects the reactants and products of the reaction. The IRC plot for the TS-II reaction path is shown in Fig. 4.

The structure of TS-II is similar to a bicycle, in which the atoms involved in the reaction changes, C2,

C9, O11, H12, and C3, are almost in a plane (dihedral angle C_2—C_9—O_{11}—H_{12}, Table X) at about 32° from the furan ring plane (dihedral C_2—C_9—O_{11}—H_{12}). The process is concerted in the sense that O11—H12 and C2—C9 bond distances increase showing breaking of these bonds, with more progress in the O11—H12 bond breaking compared to mechanism 1 (0.970–1.580 Å in TS-II for the O11—H12 bond and 1.472–1.550 Å in TS-II for the C2—C9 bond). The C9—O11 and C2—O1 bond distances reveal changes of bond order (1.361–1.280 Å in TS-II and 1.377–1.329 Å in TS-II, respectively). The distance between C3—H12 decreases indicating bond formation. The transition vector TV associated with the imaginary frequency characteristic of the TS shows that the process is dominated by the elongation of the O11—H12 bond while hydrogen H12 is being transferred from O11 to C3.

Natural bond orbital (NBO) charges for mechanism 1 are shown in Table XI. There is a redistribution of electron density in the TS compared to the reactant
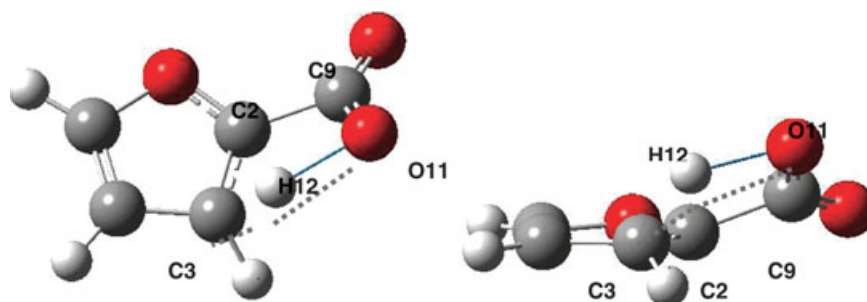

Figure 3   Two views of the five-membered TS structure found for mechanism 2, showing the transition vector. [Color figure can be viewed in the online issue, which is available at www.interscience.wiley.com.]
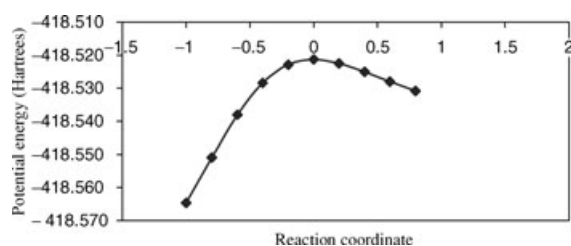
Figure 4 IRC plot for TS-II reaction path at B3LYP/6-31++G** level of theory.

furoic acid, a decrease in negative charge in O11 (from -0.705 to -0.689 in TS-I), decrease in positive charge $\delta+$ in H12 (from 0.517 to 0.431 in TS-I), an increase in negative charge in C2 (from 0.149 to -0.100 in TS-I), a decrease in negative charge in C3 (from -0.204 to -0.139 in TS-I), and an increase in positive charge in C9 (from 0.759 to 0.811 in TS-I) as the C2—C9 bond breaks and C2—H12 bond forms. The C3 atom is also involved as can be seen from the changes in electron

density, while O1 suffers small changes, implying that participation of the oxygen in the furan ring is not important.

NBO charges for mechanism 2 (TS-II) are shown in Table XII. In this case, for the analysis of NBO charges and orbital occupation for bond order calculations, we considered the zwitterion intermediate proposed for mechanism 2 (Scheme 1) as the product formed in a rate-determining step. This unstable intermediate quickly decomposes to furan and carbon dioxide.

NBO charges show a decrease in positive charge in H12 (from 0.517 to 0.429 in TS-II), increase in negative charge in C3 (from -0.204 to -0.605 in TS-II), increase in positive charge in C2 (from 0.149 to 0.484 in TS-II), and a small decrease in negative charge in O1 (from -0.473 to -0.407 in TS-II), as the zwitterion species forms while there is a almost no change for O11 in TS-II. The most significant change is the polarization of the C2—C3 bond in the sense $C2^{\delta+}$—$C3^{\delta-}$, which increases in TS-II.

Table IX Structural Parameters of 2-Furoic Acid and the Four-Membered Ring TS-I for 2-Furoic Acid Thermal Decomposition, From B3LYP/6-31++G** Calculations

	Distances (Å)				
	C_2—H_{12}	O_{11}—H_{12}	C_2—C_9	C_9—O_{11}	C_2—O_1
R	2.379	0.970	1.472	1.211	1.377
TS-I	1.274	1.441	1.630	1.288	1.404

	Dihedral Angles (deg)	
	O_1—C_2—C_9—O_{11}	C_2—C_9—O_{11}—H_{12}
TS-I	118.65	-6.03

	Imaginary Frequency (cm^{-1})
TS-I	1530.1

Table X Structural Parameters of 2-Furoic Acid and the Five-Membered Ring TS-II for 2-Furoic Acid Thermal Decomposition, From B3LYP/6-31++G** Calculations

	Distances (Å)				
	C_3—H_{12}	O_{11}—H_{12}	C_2—C_9	C_9—O_{11}	C_2—O_1	C_2—C_3
R	2.476	0.970	1.472	1.361	1.377	1.374
TS-II	1.250	1.580	1.550	1.280	1.329	1.438

	Dihedral Angles (deg)		Bond Angles (deg)	
	C_9—C_2—C_3—H_{12}	C_2—C_9—O_{11}—H_{12}	C_3—H_{12}—O_{11}	C_2—C_3—H_{12}
TS-II	31.90	2.04	131.86	85.64

	Imaginary Frequency (cm^{-1})
TS-II	1330.9

Table XI NBO Charges for Reactant R, TS, and Products P, From B3LYP/6-31++G** Calculations for Mechanism 1, Which Involves a Four-Membered Ring TS-I

Structure	C2	C3	H12	O11	C9	O1
R	0.149	−0.204	0.517	−0.705	0.759	−0.474
ET-I	−0.100	−0.139	0.431	−0.689	0.811	−0.419
P	0.090	−0.335	0.234	−0.516	1.030	−0.479

Table XII NBO Charges for Reactant R, TS, and Products P From B3LYP/6-31++G** Calculations for Mechanism 2, Which Involves a Four-Membered Ring TS-II

Structure	C2	C3	H12	O11	C9	O1
R	0.149	−0.204	0.517	−0.705	0.759	−0.473
ET-II	0.484	−0.605	0.429	−0.702	0.726	−0.407
INT	0.297	−0.646	0.287	−0.499	0.287	−0.518

Bond Order Analysis

Bond order calculations (NBO) were performed [20–22]. Wiberg bond indexes [23] were computed using the NBO program [24] as implemented in Gaussian 98W to further investigate the nature of the TS along the reaction pathway. Bond breaking and making processes involved in the reaction mechanism can be monitored by means of the synchronicity (Sy) concept proposed by Moyano et al. [25], which is defined by the expression

$$Sy = 1 - \left[\sum_{i=1}^{n} |\delta B_i - \delta B_{av}| / \delta B_{av} \right] \Big/ 2n - 2$$

where n is the number of bonds directly involved in the reaction. The relative variation of the bond index is obtained from

$$\delta B_i = \left[B_i^{TS} - B_i^{R} \right] \Big/ \left[B_i^{P} - B_i^{R} \right]$$

where the superscripts R, TS, and P represent reactant, transition state, and product, respectively.

The evolution in bond change is calculated as

$$\%Ev = \delta B_i \times 100$$

The average value is calculated from the equation

$$\delta B_{av} = 1/n \sum_{i=1}^{n} \delta Bi$$

Bonds indexes were calculated for bonds involved in the reaction changes: for (a) mechanism 1, O11−H12,

Table XIII NBO Analysis for Furoic Acid Thermal Decomposition From B3LYP/6-31++G** Calculations

Structure	O11−H12	H12−C2	C2−C9	O11−C9
δB^{R}	0.7072	0.0009	1.0370	1.0332
δB^{TS}	0.2204	0.4802	0.7542	1.3398
δB^{P}	0.0000	0.9179	0.0002	1.8888
$\%E_v$	68.8	52.3	27.3	35.8
$\delta B_{av} = 0.461$		Sy $= 0.790$		

Wiberg bond indexes (B_i), % evolution through the reaction coordinate ($\%E_v$), are shown for reactants R, TS-I, and products P. Average bond index variation (δB_{av}) and synchronicity parameter (Sy) are also reported.

Table XIV NBO Analysis for Furoic Acid Thermal Decomposition From B3LYP/6-31++G** Calculations

Structure	O11−H12	C2−C9	O11−C9	C2−C3	C3−H12
δB^{R}	0.7072	1.037	1.0332	1.5693	0.0009
δB^{TS}	0.1797	0.8852	1.3340	1.2376	0.4963
δB^{P}	0.0000	0.0006	1.8701	1.0610	1.8681
$\%E_v$	74.6	14.6	35.9	65.3	57.1
$\delta B_{av} = 0.495$		Sy $= 0.755$		

Wiberg bond indexes (B_i), % evolution through the reaction coordinate (%Ev), are shown for reactants R, TS-II, and products P. Average bond index variation (δB_{av}) and synchronicity parameter (Sy) are also reported.

H12−C2, C2−C9, and O11−C9 (TS-I, Scheme 2, Fig. 2), and (b) mechanism 2, bonds O11−H12, C2−C9, O11−C9, C2−C3, and C3−H12 (TS-II, Scheme 3, Fig. 3). All the other bonds do not undergo important changes during the process. Calculated Wiberg indexes B_i for the reactant, TS, and products for mechanisms 1 and 2 are shown in Tables XIII and XIV.

Bond order analysis revealed more progress in O11−H12 bond breaking (68%), intermediate advance in H12−C2 bond formation, and lesser progress in C2−C9 and O11−C9 bonds. A synchronicity parameter Sy of 0.79 implies a polarized asynchronic process, with late TS in the sense of H12−C2 bond formation, for mechanism 1.

Mechanism 2 is described by five reaction coordinates. In this case, Wiberg bond order indexes show more progress in O11−H12 ($\approx$75%), followed by the bond order changes in C2−C3 ($\approx$65%) and C3−H12 ($\approx$57%), moderate advance for O11−C9 ($\approx$36%), and little progress in C2−C9 bond breaking ($\approx$15%). This process is more asynchronic than mechanism 1 (Sy = 0.755), and it is also dominated by O11−H12 bond breaking.

CONCLUSIONS

The experimental data show that the elimination process of 2-furoic acid in the gas phase is homogeneous, unimolecular, and follows a first-order rate law. Theoretical calculations suggest that the reaction proceeds in a concerted asynchronous mechanism. Two concerted mechanisms were found for the thermal decomposition of 2-furoic acid. Calculated activation parameters are in better accord with mechanism 1 at the B3LYP/6-31++G** level of theory. The TS structure for mechanism 1 is a four-membered ring, where the four atoms lie in a plane forming 120° with the furan ring plane. The process is concerted polar asynchronic, dominated by the acid hydrogen transfer to the carbon bearing the carboxylic moiety in the furan ring. Mechanism 2 is described as a cyclic TS structure in which the five atoms involved are in a plane that is at about 30° to the furan ring. This process is also dominated by the breaking of the O—H bond of the acid moiety and concerted polar in nature. An experimental log A of 13.28 suggests that the reaction is likely to occur through a four-membered-ring type of mechanism. Additionally, the formation of the zwitterion species in the gas phase is unlikely because it cannot be stabilized by solvent interactions. The small negative value of the entropy of activation suggests loose polar TS. These arguments favor mechanism 1; however, mechanism 2 is not ruled out. NBO analysis suggests that the polarization of the O—H bond is the determining factor in the decomposition process and implies a polar asynchronic process. A reasonable agreement is achieved between the theoretical and experimental results.

BIBLIOGRAPHY

1. Safont, V. S.; Moliner, V.; Andres, J.; Domingo, L. R. J Phys Chem A 1997, 101, 1859.
2. Domingo, L. R.; Andres, J.; Moliner, V.; Safont, V. S. J Am Chem Soc 1997, 119, 6415.
3. Domingo, L. R.; Pitcher, M. T.; Andres, J.; Moliner, V.; Safont, V. S.; Chuchani, G. Chem Phys Lett 1997, 274, 422.
4. Domingo, L. R.; Pitcher, M. T.; Safont, V.; Andres, J.; Chuchani, G. J Phys Chem A 1999, 103, 3935.
5. Rotinov, A.; Chuchani, G.; Andres, J.; Domingo, L. R.; Safont, V. S. Chem Phys 1999, 246, 1.
6. Chuchani, G.; Domínguez, R. M.; Rotinov, A.; Martín, I. J Phys Org Chem 1999, 12, 612.
7. Chuchani, G.; Domínguez, R. M.; Herize, A.; Romero, R. J Phys Org Chem 2000, 13, 757.
8. Ensuncho, A.; Lafont, J.; Rotinov, A.; Domínguez, R. M.; Herize, A.; Quijano, J.; Chuchani, G. Int J Chem Kinetic 2000, 33, 465, and references cited therein.
9. Dominguez, R. M.; Tosta, M.; Chuchani, G. J Phys Org Chem 2003, 16, 869.
10. Lafont, J.; Ensuncho, A.; Dominguez, R. M.; Rotinov, A.; Herize, A.; Quijano, J.; Chuchani, G. J Phys Org Chem 2003, 16, 84.
11. Maccoll, A. J Chem Soc 1955, 965.
12. Swinbourne, E. S. Aust J Chem 1958, 11, 314.
13. Dominguez, R. M.; Herize, A.; Rotinov, A.; Alvarez-Aular, A.; Visbal, G.; Chuchani, G. J Phys Org Chem 2004, 17, 399.
14. Frisch, M. J.; Trucks, G. W.; Schlegel, H. B.; Scuseria, G. E.; Robb, M. A.; Cheeseman, J. R.; Zakrzewski, V. G.; Montgomery, J. A., Jr.; Stratmann, R. E.; Burant, J. C.; Dapprich, S.; Millam, J. M.; Daniels, A. D.; Kudin, K. N.; Strain, M. C.; Farkas, O.; Tomasi, J.; Barone, V.; Cossi, M.; Cammi, R.; Mennucci, B.; Pomelli, C.; Adamo, C.; Clifford, S.; Ochterski, J.; Petersson, G. A.; Ayala, P. Y.; Cui, Q.; Morokuma, K.; Malick, D. K.; Rabuck, A. D.; Raghavachari, K.; Foresman, J. B.; Cioslowski, J.; Ortiz, J. V.; Stefanov, B. B.; Liu, G.; Liashenko, A.; Piskorz, P.; Komaromi, I.; Gomperts, R.; Martin, R. L.; Fox, D. J.; Keith, T.; Al-Laham, M. A.; Peng, C. Y.; Nanayakkara, A.; Gonzalez, C.; Challacombe, M.; Gill, P. M. W.; Johnson, B.; Chen, W.; Wong, M. W.; Andres, J. L.; Gonzalez, C.; Head-Gordon, M.; Replogle, E. S.; Pople, J. A. Gaussian 98, Revision A.3; Gaussian, Inc.: Pittsburgh, PA, 1998.
15. McQuarrie, D. Statistical Mechanics; Harper & Row: New York, 1986.
16. Foresman, J. B.; Frish, Æ. Exploring Chemistry with Electronic Methods, 2nd ed.; Gaussian, Inc: Pittsburgh, PA, 1996.
17. Rotinov, A.; Dominguez, R. M.; Córdova, T.; Chuchani, G. J Phys Org Chem 2005, 18, 616.
18. Benson, S. W. The Foundations of Chemical Kinetics; Mc-Graw-Hill: New York, 1960.
19. O'Neal, H. E.; Benson, S. W. J Phys Chem 1967, 71, 2903; Benson, S. B. Thermochemical Kinetics; John Wiley & Sons: New York, 1968.
20. Lendvay, G. J Phys Chem 1989, 93, 4422.
21. Reed, A. E.; Weinstock, R. B.; Weinhold, F. J Chem Phys 1985, 83(2), 735.
22. Reed, A. E.; Curtiss, L. A.; Weinhold, F. Chem Rev 1988, 88, 899.
23. Wiberg, K. B. Tetrahedron 1968, 24, 1083.
24. Gaussian NBO, version 3.1.
25. Moyano, A.; Periclas, M. A.; Valenti, E. J Org Chem 1989, 54, 573.